EULERIAN MOMENT EQUATIONS FOR 2-D STOCHASTIC IMMISCIBLE FLOW

KENNETH D. JARMAN* AND THOMAS F. RUSSELL†

Abstract. We solve statistical moment differential equations (MDEs) for immiscible flow in porous media in the limit of zero capillary pressure, with application to secondary oil recovery. Closure is achieved by Taylor expansion of the fractional flow function and a perturbation argument. Previous results in 1-D are extended to 2-D, in which a bimodal profile is less evident.

Mean and variance of (water) saturation exhibit a bimodal character; two shocks replace the single shock front evident in the classical Buckley–Leverett saturation profile. Comparison to Monte Carlo simulations (MCS) shows that the MDE approach gives a good approximation to total oil production. For such integrated or averaged quantities, or where a rough approximation of the location and magnitude of uncertainty is sufficient, MDEs may be substantially more efficient than MCS.

Key words. porous media, stochastic, random fields, moment equations

AMS subject classifications. 76T99, 76S05, 35L60, 35L65

1. Introduction.

Stochastic representations of subsurface geologic properties have become commonplace due to the difficulty in complete and certain characterization of these properties. This leads to uncertainty in flow profiles in such porous media, so that statistical description of outcomes is appropriate. Additionally, from the perspective of practical macroscopic field-scale models, microscopic heterogeneities and flows can be viewed as random processes to be upscaled. In two-phase flow on a field scale, we are primarily interested in mean behavior and a measure of uncertainty in the saturation of each phase, which can be a measure of "macrodispersion" in certain upscaling contexts.

A "zeroth-order" model of mean flow with averages of geologic properties ignores correlations between flow variables. Monte Carlo simulations (MCS) of many realizations of geologic properties to estimate moments require much computation time and careful sampling techniques [10, 11, 29]. Macrodispersion theory in contaminant transport captures an approximate effect of fluctuations by modeling covariance functions in an equation for the mean concentration [5, 12]. This theory has a long history in subsurface contaminant transport and is closely related to eddy diffusion models of turbulence [15, p. 358 ff].

Rather than approximate covariance functions as macrodispersive terms, which requires neglecting fluctuations in second moments, we solve PDEs for the covariance functions and the mean of saturation, extending previous results to 2-D. These *moment differential equations* (MDEs) are derived using a modified perturbation expansion as described in [17]. The MDEs allow direct approximation of the local mean and covariance functions for general boundary conditions and general, nonstationary stochastic geology [33].

*Computational Sciences and Mathematics Division, Fundamental Science Directorate, Pacific Northwest National Laboratory, P.O. Box 999 / MS K1-85, Richland, Washington 99352 (kj@pnl.gov). Supported by NSF Graduate Traineeship in Applied Mathematics (DMS-9208685) and DOE Laboratory Directed Research and Development.

†Department of Mathematics, University of Colorado at Denver, P.O. Box 173364, Campus Box 170, Denver, Colorado 80217-3364 (trussell@math.cudenver.edu). Supported in part by NSF Grant Nos. DMS-9706866, DMS-0084438 and DMS-0222300, and ARO Grant No. DAAG55-97-1-0171.

Report Documentation Page

Form Approved
OMB No. 0704-0188

1. REPORT DATE	2. REPORT TYPE	3. DATES COVERED
2006		**00-00-2006 to 00-00-2006**

4. TITLE AND SUBTITLE	5a. CONTRACT NUMBER
Eulerian Moment Equations for 2-D Stochastic Immiscible Flow	5b. GRANT NUMBER
	5c. PROGRAM ELEMENT NUMBER
6. AUTHOR(S)	5d. PROJECT NUMBER
	5e. TASK NUMBER
	5f. WORK UNIT NUMBER
7. PERFORMING ORGANIZATION NAME(S) AND ADDRESS(ES) **Pacifica Northwest National Laboratory,Computational Sciences and Mathematics Division,PO Box 999,Richland ,WA,99352**	8. PERFORMING ORGANIZATION REPORT NUMBER
9. SPONSORING/MONITORING AGENCY NAME(S) AND ADDRESS(ES)	10. SPONSOR/MONITOR'S ACRONYM(S)
	11. SPONSOR/MONITOR'S REPORT NUMBER(S)

12. DISTRIBUTION/AVAILABILITY STATEMENT
Approved for public release; distribution unlimited

13. SUPPLEMENTARY NOTES

14. ABSTRACT
see report

15. SUBJECT TERMS

16. SECURITY CLASSIFICATION OF:			17. LIMITATION OF ABSTRACT	18. NUMBER OF PAGES	19a. NAME OF RESPONSIBLE PERSON
a. REPORT	b. ABSTRACT	c. THIS PAGE			
unclassified	**unclassified**	**unclassified**		**18**	

1.1. Applications. A statistical description of subsurface flow is of particular interest for secondary oil recovery. In the advection equation, the principal difficulty is a non-convex nonlinear flux function that leads to discontinuous solutions. Standard pressure-saturation equations for 2-D horizontal flow of two incompressible immiscible fluids in porous media in the limit of vanishing capillary pressure ($p_c = 0$) are

$$\phi\,\mathbf{v}(\mathbf{x}) = -\mathbf{K}(\mathbf{x})\,\nabla h(\mathbf{x}), \qquad \nabla\cdot\mathbf{v}(\mathbf{x}) = 0, \tag{1.1}$$

$$\partial_t s(\mathbf{x},t) + \nabla\cdot[f(s(\mathbf{x},t))\mathbf{v}(\mathbf{x})] = 0. \tag{1.2}$$

These are considered valid from *laboratory* (centimeters) to *field* scales of reservoir depth (10–100 meters) and length (100–10,000 meters). Hydraulic conductivity $\mathbf{K}$ may be an anisotropic tensor; here, for simplicity, it will be an isotropic scalar K. Assume also that K depends weakly on (water) saturation s $[1,3]$. Apply (1.1)–(1.2) to the flow of oil and water, for arbitrary fluid mobilities. Denote the *total velocity*, a scaled total volumetric flux of both fluids, by $\mathbf{v}$, hydraulic water head by h, and porosity (assumed constant) by ϕ. The *fractional flow function* $f(s)$, for $p_c = 0$, represents the fraction of $\mathbf{v}$ due to water. It is typically S-shaped as shown in Fig. 1.1; in §4.1 we use a form arising from quadratic relative permeabilities (see [1]). However, our method does not depend on any such specific choice of $f(s)$.

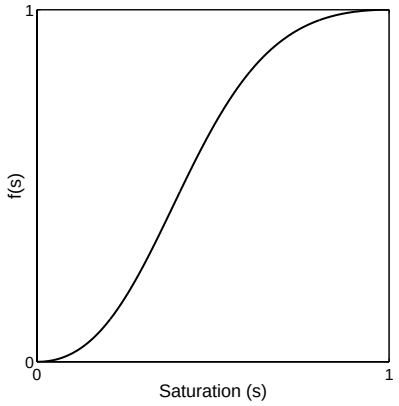

FIG. 1.1. *The nonconvex fractional flow function.*

Capillary pressure regularizes sharp fronts caused by the nonlinear advection term. To obtain a linear approximation to this effect, add $\epsilon_D\nabla^2 s(\mathbf{x},t)$ with $\epsilon_D > 0$ to the right side of (1.2). Letting $\epsilon_D \to 0$ defines the *vanishing-viscosity* solution [27], which is the one we seek.

As is standard in subsurface applications, let $Y = \ln K$ be a random field with prescribed mean and covariance functions; e.g., it is often claimed that Y is multivariate Gaussian, based on empirical observations [8] (again our method does not depend on such a limiting assumption). Through (1.1)–(1.2), $\mathbf{v}$ and s are thus random fields. No other underlying sources of uncertainty are considered in this study.

Under the assumptions stated above, with steady boundary conditions, and neglecting the weak dependence of K on s, a steady $\mathbf{v}$ can be determined from (1.1). We evolve s from the stochastic PDE (1.2), assuming known statistics of $\mathbf{v}$. Moments of $\mathbf{v}$ and h can be estimated from established theory ([31–33, 36] use MDEs). We

combine analytical and numerical techniques to model the propagation of uncertainty from an underlying random field $Y(\mathbf{x})$, through $\mathbf{v}(\mathbf{x})$ to the solution $s(\mathbf{x}, t)$.

1.2. Previous work. Existing work on MDEs focuses mostly on advection equations with linear flux functions [13] and some nonlinear subsurface flow equations of a form different from (1.2) [2, 28, 31, 32, 36].

Langlo and Espedal [19, 20] present a macrodispersion approach for the stochastic version of (1.2). The flux function is expanded in a Taylor series, and high-order terms are neglected; then standard techniques represent macrodispersivity as a function of flow velocity covariance. Zhang, Tchelepi, and Li take advantage of the steady velocity field, and transform 2-D flow to 1-D Lagrangian flow along streamlines [34, 35]. They formulate integral equations for moments from ensemble averages over the streamlines rather than a system of MDEs. Variations on the streamline approach are currently popular in stochastic subsurface hydrology [4, 6, 7, 25, 26].

An Eulerian MDE approach has been successful for single- and multiphase pressure and velocity equations [31], and a natural next step is to extend the theory from flux equations to transport equations (as in [13]) and (1.2). The Eulerian framework differs from streamlines not only in formulation but also in that the MDEs need no velocity-distribution assumption and extension to transient velocity fields is relatively straightforward. The appeal of MDEs relative to macrodispersion approaches is that covariances are computed directly, so that it is not necessary to approximate them by solving an approximate fluctuation equation that neglects second-moment fluctuations. In [17] and [18], we derived and solved second-order MDEs for (1.2) in 1-D, using three different perturbation approaches. One of these approaches, a modified expansion described in [17], is applied here in 2-D.

Equations are presented in §2. In §3, we discuss classification of MDEs and the fundamental difference between 2-D and 1-D MDEs. Numerical solutions are given in §4 and are compared to Monte Carlo simulations.

2. Moment Equations. We use a modified perturbation expansion, described in detail in [17], to derive statistical MDEs. Closure implicitly depends upon the assumption that random fluctuations in $Y = \ln K$ are small ($\sigma_Y \ll 1$). Moments of h and $\mathbf{v}$ are assumed known from (1.1) and moments of Y.

The saturation equation (1.2), with initial data $s(\mathbf{x}, 0) = g(\mathbf{x})$, is

$$\partial_t s + \partial_{x_i}(f(s)v_i) = 0 \tag{2.1}$$

(Einstein summation convention assumed). We assume that g is known with certainty. Solutions are defined in terms of vanishing viscosity as in §1.1; henceforth, this is tacitly understood.

For examples of commonly used methods for deriving moment equations with applications to subsurface flow and transport, see [5, 9, 12, 13, 23, 31]. These methods originated in the correlation equations of turbulence models. Here we apply a modification to a standard asymptotic expansion.

Let $\langle\cdot\rangle$ denote the expectation operator, defined by

$$\langle\psi\rangle \equiv \int_\Omega \psi(\omega)\, dP(\omega) \tag{2.2}$$

for any integrable function $\psi : \Omega \to \mathbb{R}$ on the sample space Ω with probability measure P. We omit reference to ω in what follows.

The random field Y is decomposed into deterministic mean plus random fluctuation: $Y = \langle Y \rangle + \delta Y$. Each field dependent on Y is represented by a formal power expansion in an as-yet unknown parameter ϵ:

$$h = \sum_{n=0}^{\infty} \epsilon^n h_n(\mathbf{x}), \quad \mathbf{v} = \sum_{n=0}^{\infty} \epsilon^n \mathbf{v}_n(\mathbf{x}), \quad s = \sum_{n=0}^{\infty} \epsilon^n s_n(\mathbf{x}, t). \tag{2.3}$$

The expansion parameter $\epsilon = \sigma_Y$ is shown to be appropriate within the context of the velocity and head equations (1.1) [5, pp. 184–190], [33]. For example, for single-phase, stationary uniform mean flow on an infinite domain in 1-D, v_0 is a deterministic scalar and σ_v^2 is shown to be approximated by $\epsilon^2 \left\langle v_1^2 \right\rangle = v_0^2 \sigma_Y^2$. In 2-D, we denote the components of $\mathbf{v}_n$ by $(v_i)_n$ for $i = 1, 2$.

In the following, the term "order" applies to the power of ϵ rather than the order of the statistical moment. In special cases, we may use the term "order" in the latter sense and clearly differentiate from order in ϵ. Thus, a "second moment" is a covariance, but "second-order moment" is any moment that is approximated to order ϵ^2. Recall that we only need the decompositions of $\mathbf{v}$ and s here. The fractional flow function is expanded in a Taylor series around $\tilde{s} = s_0 + \epsilon \langle s_1 \rangle + \epsilon^2 \langle s_2 \rangle$ (a second-order approximation to the mean saturation; we see below that $\langle s_0 \rangle = s_0$):

$$f(s) = f(\tilde{s}) + f'(\tilde{s})(s - \tilde{s}) + \frac{1}{2} f''(\tilde{s})(s - \tilde{s})^2 + \cdots, \tag{2.4}$$

where

$$s - \tilde{s} = \delta s_0 + \epsilon \delta s_1 + \epsilon^2 \delta s_2 + \sum_{n=3}^{\infty} \epsilon^n s_n(\mathbf{x}, t).$$

The expansion center $\tilde{s}$ is our approximation to the mean saturation, so we retain $\tilde{s}$ as the argument of f in the following modification to the standard equations of order $0, 1$, and 2. The modified equations for s_0 and s_1, obtained by substituting (2.3) and (2.4) into (2.1) and collecting the powers ϵ^0 and ϵ^1, are given by

$$\partial_t s_0 + \partial_{x_i} [f(\tilde{s})(v_i)_0] = 0, \tag{2.5}$$

and

$$\partial_t s_1 + \partial_{x_i} \Big[f(\tilde{s})(v_i)_1 + f'(\tilde{s}) \delta s_1 (v_i)_0 \Big] = 0. \tag{2.6}$$

Note that $\langle s_0 \rangle = s_0$, because all other terms in the equation for s_0 are deterministic. We show that $\langle s_1 \rangle = 0$. By definition, $\langle \delta s_1 \rangle = 0$. Also, $\langle \mathbf{v}_1 \rangle = \mathbf{0}$ by a standard result from the theory for moment equations of multidimensional single-phase flow [36]. Applying the expectation operator $\langle \cdot \rangle$ to the first-order equation (2.6) gives

$$0 = \partial_t \langle s_1 \rangle + \partial_{x_i} \Big[f(\tilde{s}) \langle (v_i)_1 \rangle + f'(\tilde{s}) \langle \delta s_1 \rangle (v_i)_0 \Big] = \partial_t \langle s_1 \rangle . \tag{2.7}$$

The initial data are deterministic; therefore, $\langle s_1 \rangle$ is initially zero, and (2.7) implies that $\langle s_1 \rangle$ remains zero for all time. The mean approximation is then $\tilde{s} = s_0 + \epsilon^2 \langle s_2 \rangle$. The correction term s_2 satisfies

$$\partial_t s_2 + \partial_{x_i} \Big[f(\tilde{s})(v_i)_2 + f'(\tilde{s}) \delta s_1 (v_i)_1 + f'(\tilde{s}) \delta s_2 (v_i)_0 + \frac{1}{2} f''(\tilde{s}) \delta {s_1}^2 (v_i)_0 \Big] = 0.$$

Apply the expectation operator and note that $\langle \delta {s_1}^2 \rangle = \langle s_1 s_1 \rangle - \langle s_1 \rangle \langle s_1 \rangle = \langle {s_1}^2 \rangle$, $\langle \delta s_2 \rangle = 0$, and $\mathbf{v}_1 = \delta \mathbf{v}_1$ implies $\langle \delta s_1 (v_i)_1 \rangle = \langle \delta s_1 (\delta v_i)_1 \rangle = \langle s_1 (v_i)_1 \rangle - \langle s_1 \rangle \langle (v_i)_1 \rangle = \langle s_1 (v_i)_1 \rangle$, to obtain the following correction to (2.5):

$$\partial_t \langle s_2 \rangle + \partial_{x_i} \Big[f(\tilde{s}) \langle (v_i)_2 \rangle + f'(\tilde{s}) \langle s_1 (v_i)_1 \rangle + \frac{1}{2} f''(\tilde{s}) \langle {s_1}^2 \rangle (v_i)_0 \Big] = 0. \tag{2.8}$$

Define $\tilde{\mathbf{v}} = \mathbf{v}_0 + \epsilon^2 \langle \mathbf{v}_2 \rangle$, which is consistent with the second-order theory for single-phase flow. Adding the zeroth-order equation (2.5) to $\epsilon^2 \times$(2.8) gives an equation for the mean saturation:

$$\partial_t \tilde{s} + \partial_{x_i} \Big[f(\tilde{s}) \tilde{v}_i + \epsilon^2 f'(\tilde{s}) \langle s_1 (v_i)_1 \rangle + \frac{\epsilon^2}{2} f''(\tilde{s}) \langle {s_1}^2 \rangle (v_i)_0 \Big] = 0. \tag{2.9}$$

We derive equations for the unknown covariance functions $\langle s_1 (v_i)_1 \rangle$ and $\langle s_1^2 \rangle$ using the following additional notation. The independent variables are $\mathbf{x}$ and t except where noted, and $\cdot|_{\mathbf{y}}$ denotes the replacement of $\mathbf{x}$ by some $\mathbf{y}$ different from $\mathbf{x}$. It is convenient and useful to derive equations for the more general two-point covariances $\langle s_1 (v_i)_1 |_{\mathbf{y}} \rangle$ and $\langle s_1 s_1 |_{\mathbf{y}} \rangle$ rather than for one-point covariances.

To obtain an equation for $\langle s_1 (v_i)_1 |_{\mathbf{y}} \rangle$, multiply (2.6) by $(v_i)_1(\mathbf{y})$, and apply $\langle \cdot \rangle$. This results in

$$\partial_t \langle s_1 (v_i)_1 |_{\mathbf{y}} \rangle + \partial_{x_i} \Big[f(\tilde{s}) \langle (v_i)_1 (v_i)_1 |_{\mathbf{y}} \rangle + f'(\tilde{s}) (v_i)_0 \langle s_1 (v_i)_1 |_{\mathbf{y}} \rangle \Big] = 0. \tag{2.10}$$

Similarly, multiply (2.6) by $s_1(\mathbf{y}, t)$ and use the identity[1] $s_1|_{\mathbf{y}} \partial_t s_1 = \partial_t (s_1 s_1|_{\mathbf{y}}) - s_1 \partial_t s_1|_{\mathbf{y}}$, then use (2.6) with $\mathbf{y}$ in place of $\mathbf{x}$, yielding this equation for the two-point saturation covariance:

$$\begin{aligned} &\partial_t \langle s_1 s_1 |_{\mathbf{y}} \rangle + \partial_{x_i} \Big[f(\tilde{s}) \langle s_1 |_{\mathbf{y}} (v_i)_1 \rangle + f'(\tilde{s}) (v_i)_0 \langle s_1 s_1 |_{\mathbf{y}} \rangle \Big] \\ &+ \partial_{y_i} \Big[f(\tilde{s}|_{\mathbf{y}}) \langle s_1 (v_i)_1 |_{\mathbf{y}} \rangle + f'(\tilde{s}|_{\mathbf{y}}) (v_i)_0|_{\mathbf{y}} \langle s_1 |_{\mathbf{y}} s_1 \rangle \Big] = 0. \end{aligned} \tag{2.11}$$

Define $c_{sv_i}(\mathbf{x}, \mathbf{y}, t) = \epsilon^2 \langle s_1 (v_i)_1 |_{\mathbf{y}} \rangle$, $c_s = \epsilon^2 \langle s_1 s_1 |_{\mathbf{y}} \rangle$, $c_{v_i v_j} = \epsilon^2 \langle (v_i)_1 (v_j)_1 |_{\mathbf{y}} \rangle$, $\langle s \rangle |_{\mathbf{y}} = \langle s \rangle (\mathbf{y}, t)$, $\sigma_{sv_i}(\mathbf{x}, t) = c_{sv_i}(\mathbf{x}, \mathbf{x}, t)$, and $\sigma_s^2(\mathbf{x}, t) = c_s(\mathbf{x}, \mathbf{x}, t)$. Let a caret over a variable denote the mapping $\widehat{\psi}(\mathbf{x}, \mathbf{y}, t) = \psi(\mathbf{y}, \mathbf{x}, t)$ for any function ψ. The resulting system is

$$\partial_t \tilde{s} + \partial_{x_i} \Big[f(\tilde{s}) \tilde{v}_i + f'(\tilde{s}) \sigma_{sv_i} + \frac{1}{2} f''(\tilde{s}) (v_i)_0 \, \sigma_s^2 \Big] = 0, \tag{2.12a}$$

$$\partial_t c_{sv_j} + \partial_{x_i} \Big[f(\tilde{s}) c_{v_i v_j} + f'(\tilde{s}) (v_i)_0 \, c_{sv_j} \Big] = 0, \tag{2.12b}$$

$$\partial_t c_s + \partial_{x_i} \Big[f(\tilde{s}) \widehat{c}_{sv_i} + f'(\tilde{s}) (v_i)_0 c_s \Big] + \partial_{y_i} \Big[f\big(\widehat{\tilde{s}}\big) c_{sv_i} + f'\big(\widehat{\tilde{s}}\big) (v_i)_0|_{\mathbf{y}} c_s \Big] = 0; \tag{2.12c}$$

$$i, j = 1, 2.$$

Recall that velocity moments $(v_i)_0$, $\tilde{v}_i$, and $c_{v_i v_j}$ are assumed known. The flux in (2.12a) consists of a nonlinear advective mean flux term and two covariance terms. In turbulence applications, terms such as c_{sv_j} often are referred to as transport by fluctuations [22]. Both (2.12b) and (2.12c) have advective flux terms, are coupled to

[1] The identity is not valid in a strong sense for discontinuous solutions. Recall, however, that we define solutions in terms of the (smooth) viscous solution, in the limit $\epsilon_D \to 0$.

the mean equation (2.12a), and are first-order in $\epsilon^2 = \sigma_Y^2$. This is consistent with the approximation $\tilde{s}$, which is second-order in σ_Y. However, due to the choice of $\tilde{s}$, higher-order effects are included in (2.12). We demonstrate this fact for the case $f(s) = s$, where the mean advective flux term in (2.12a) is $\partial_{x_i}[\tilde{s}\tilde{v}_i]$, or $\partial_{x_i}[(s_0 + \epsilon^2 \langle s_2 \rangle)((v_i)_0 + \epsilon^2 \langle (v_i)_2 \rangle)]$. The term $\epsilon^4 \partial_{x_i}[\langle s_2 \rangle \langle (v_i)_2 \rangle]$ in this expression is a partial fourth-order correction.

We refer to this problem as 2-D although the covariance functions involve four spatial variables and the saturation covariance has fluxes in all directions. The four variables represent two different points in the same 2-D domain.

To formally define the vanishing-viscosity solution, first add the deterministic term $\epsilon_D \partial_{x_i}^2 s$ to (2.1) and carry out the expansion and derivation above. This adds diffusion terms $\epsilon_D \partial_{x_i}^2 \tilde{s}$, $\epsilon_D \partial_{x_i}^2 c_{sv_j}$, and $\epsilon_D \partial_{x_i}^2 c_s$ to the right-hand sides of (2.12a), (2.12b), and (2.12c), respectively. Then find solutions in the limit $\epsilon_D \to 0$. In practice we solve the system (2.12) directly.

3. Classification. Classification is of interest for several reasons. Macrodispersion theory produces a parabolic equation for the mean, with a macrodispersivity that depends on $c_{v_i v_j}$ and $\langle s \rangle$. In contrast, we have shown that 1-D MDEs are hyperbolic [18]. To achieve this result, we exploited special structure to reduce the equations. Namely, 1-D velocity has an infinite correlation length because it is a spatially constant random variable. This led to the covariance relationship $c_s \; c_v = c_{sv} \; \widehat{c}_{sv}$. Velocity correlations have a finite length scale in 2-D. We argue that this fact prohibits classification and suggests a transition to parabolic behavior as described by macrodispersion theory.

We expect the equations to be nearly hyperbolic since the original deterministic PDE (1.2) is hyperbolic. However, σ_{sv_i} and σ_s^2, rather than c_{sv_i} and c_s, appear in the mean equation. This mix of one-point and two-point covariance functions prevents us from immediately treating the MDEs as classically hyperbolic. Also, independent variables $\mathbf{x}$ and $\mathbf{y}$ are permuted in $\tilde{s}$ and c_{sv_j} in (2.12c). In general, $\tilde{s}|_{\mathbf{y}} = \tilde{s}(\mathbf{y}, t) \neq \tilde{s}(\mathbf{x}, t)$, and $\widehat{c}_{sv_j} \neq c_{sv_j}$. The system (2.12) cannot even be written in conservation-law form. The inconsistency in independent variables is dealt with directly by writing a redundant set of equations for the functions $\widehat{\tilde{s}}$ and $\widehat{c}_{sv_j}$.

Transposing $\mathbf{x}$ and $\mathbf{y}$ in (2.12a) and (2.12b) results in the expanded system

$$
\begin{aligned}
\partial_t \tilde{s} + \partial_{x_i}\Big[f(\tilde{s})\tilde{v}_i + f'(\tilde{s})\sigma_{sv_i} + \frac{1}{2} f''(\tilde{s})(v_i)_0 \sigma_s^2\Big] &= 0, \\
\partial_t c_{sv_j} + \partial_{x_i}\Big[f(\tilde{s}) c_{v_i v_j} + f'(\tilde{s})(v_i)_0 c_{sv_j}\Big] &= 0, \\
\partial_t c_s + \partial_{x_i}\Big[f(\tilde{s})\widehat{c}_{sv_i} + f'(\tilde{s})(v_i)_0 c_s\Big] + \partial_{y_i}\Big[f\big(\widehat{\tilde{s}}\big) c_{sv_i} + f'\big(\widehat{\tilde{s}}\big)(v_i)_0|_{\mathbf{y}} c_s\Big] &= 0, \qquad (3.1) \\
\partial_t \widehat{c}_{sv_j} + \partial_{y_i}\Big[f\big(\widehat{\tilde{s}}\big) c_{v_j v_i} + f'\big(\widehat{\tilde{s}}\big)(v_i)_0|_{\mathbf{y}} \widehat{c}_{sv_j}\Big] &= 0, \\
\partial_t \widehat{\tilde{s}} + \partial_{y_i}\Big[f\big(\widehat{\tilde{s}}\big)\tilde{v}_i|_{\mathbf{y}} + f'\big(\widehat{\tilde{s}}\big)\widehat{\sigma}_{sv_i} + \frac{1}{2} f''\big(\widehat{\tilde{s}}\big)(v_i)_0|_{\mathbf{y}} \widehat{\sigma}_s^2\Big] &= 0;
\end{aligned}
$$

with $i, j = 1, 2$, where $\widehat{\sigma}_{sv_i}(\mathbf{y}, t) = c_{sv_i}(\mathbf{y}, \mathbf{y}, t)$, $\widehat{\sigma}_s^2(\mathbf{y}, t) = c_s(\mathbf{y}, \mathbf{y}, t)$. The system is symmetric under the permutation $\widehat{\psi}(\mathbf{x}, \mathbf{y}, t) = \psi(\mathbf{y}, \mathbf{x}, t)$. To be consistent with the original system (2.12a)–(2.12c), the initial conditions and the numerical method must obey this symmetry.

4. Solution. We numerically solve (3.1) with a first-order upwind scheme within the framework of CLAWPACK [21]. However, we do not take full advantage of the

functionality of CLAWPACK due to the difficulty in defining a Riemann solver for the MDEs. The solutions are shown to be bimodal as in 1-D (see Fig. 4.1, and see [18] for 1-D details). Solutions are also compared to MCS moment estimates.

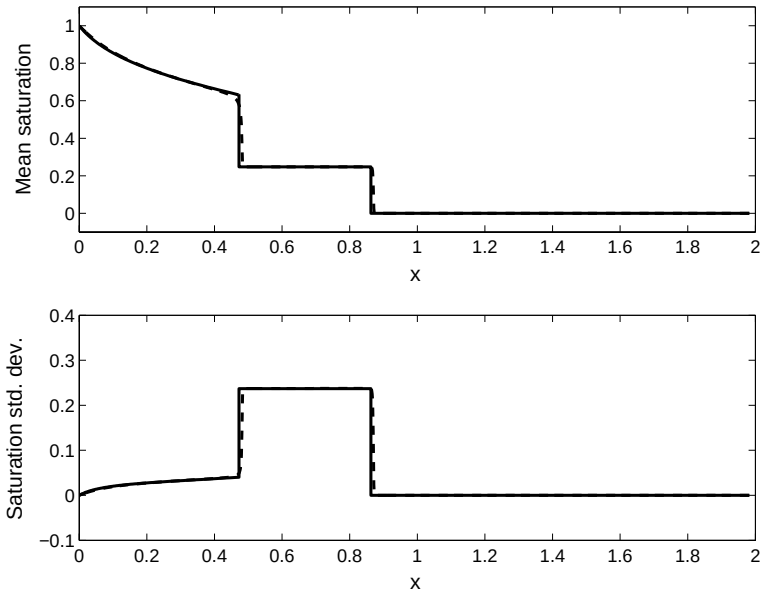

FIG. 4.1. *Mean and standard deviation of saturation (1-D). The solid curve is a semi-analytical solution described in [18]; dashed curve is obtained from fine-grid numerical PDE scheme.*

4.1. MDEs. Our example problem is on a rectangular domain $R = [0, L_1] \times [0, L_2] = [0, 2] \times [0, 1]$, $\mathbf{x} = (x_1, x_2) \in R$, with $\partial_{x_2} h(\mathbf{x}) = 0$ on $x_2 = 0$ and $x_2 = 1$ and constant $h(\mathbf{x})$ at $x_1 = 0$ and $x_1 = 2$. The entire domain R is initially oil-saturated ($s = 0$), with water ($s = 1$) pumped in along $x_1 = 0$. We choose a form of the fractional flow function $f(s)$ that arises from quadratic relative permeabilities: $f(s) = s^2/(s^2 + m(1 - s)^2)$. We set the *viscosity ratio* m to 0.5 and porosity ϕ to 0.2. Statistical parameters for MDEs are $\langle Y \rangle = 0$ and $\sigma_Y^2 = 0.25$, and we use the exponential covariance function given by

$$C(\mathbf{r}) = \sigma_Y^2 \exp\left[-\frac{|r_1|}{\lambda_1} - \frac{|r_2|}{\lambda_2}\right], \tag{4.1}$$

where $\mathbf{r} = (r_1, r_2)$. We set correlation lengths $\lambda_1 = \lambda_2 = 0.2$. This gives 5 correlation lengths in the x_2 direction and 10 correlation lengths in the x_1 direction. Hydraulic head and velocity moments were computed using the semi-analytical flow approach of Zhang and Winter [30, 36]. The authors derived MDEs using perturbation expansions in a manner similar to ours. Due to the mathematical complexity caused by the presence of boundaries and nonstationarity, these MDEs are solved numerically. Finite velocity correlation length is evident in examples of velocity covariance shown in Fig. 4.2.

We use a very coarse grid (40 by 20) due to the fact that two-point covariance functions make the 2-D MDEs essentially 4-D. The 2-D solutions for the mean $\tilde{s}$ and variance σ_s^2 of saturation are shown at an early and late time in Fig. 4.3. These indicate a pair of saturation fronts moving at distinct speeds. Saturation-velocity

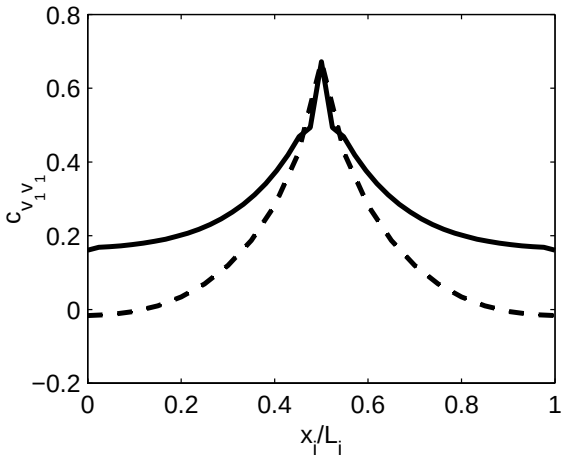

FIG. 4.2. *Velocity covariance $c_{v_1v_1}$, showing finite correlation length. The solid line shows covariance between v_1 at the center of the domain and at all points on $x_2 = L_2/2$. The dotted line shows covariance between v_1 at the center and at all points along $x_1 = L_1/2$.*

one-point covariances σ_{sv_i}, $i = 1, 2$ are shown in Fig. 4.4. The σ_{sv_1} surface is similar to that of σ_s^2, and is very close to the 1-D profile.

The results also are shown for $\tilde{s}$, σ_{sv_1}, and σ_s along a slice at $x_2 = L_2/4$ on the longitudinal axis in Fig. 4.5. In each case, a bimodal solution is evident. On the left, a rarefaction zone trails a slow front. Physically this represents a smoothly varying mixture of two phases. The uncertainty as measured by σ_s^2 is relatively small in this region. Beyond the slow front, in the interval of uncertainty, there is a nearly constant ratio of phases. Finally, at the fast front, mean saturation and covariances drop to zero; beyond the front, only one phase (oil) is present.

A crude test now can be performed to see whether a covariance relationship holds similar to that in 1-D. The flow is nearly 1-D; transverse velocities are much smaller than longitudinal velocities, and σ_{sv_2} is much smaller than σ_{sv_1}. So it is reasonable to expect that the products $\sigma_s^2\sigma_{v_1v_1}$ and $\sigma_{sv_1}^2$ are similar, because they are identical in 1-D. However, observe the dip in σ_{sv_1} between two peaks (Fig. 4.5), on the interval of uncertainty. The saturation variance does not have such a profile, and neither does $\sigma_{v_1v_1}$ (see Appendix A). Thus there is a difference in shape between the two products $\sigma_s^2\sigma_{v_1v_1}$ and $\sigma_{sv_1}^2$, so that the 1-D identity $\sigma_s^2\sigma_{v_1v_1} = \sigma_{sv_1}^2$ cannot hold.

The 2-D solutions are comparable to solutions in the limit of 1-D flow. This limiting solution is obtained by letting the longitudinal velocity components $\tilde{v}_1$, $(v_1)_0$ be constant and setting transverse velocities to zero. The limiting solution matches a 1-D solution computed on the coarse grid. The result along a longitudinal slice is shown in Fig. 4.6. (The 1-D result is diffused compared to Fig. 4.1 because of the coarse grid.) The nearly uniform 2-D flow scenario chosen gives results nearly identical to those in 1-D in spite of the localized velocity correlation structure in 2-D.

The addition of small linear diffusion terms, which are employed in the numerical scheme to stabilize the solution, does not eliminate bimodality. The fact that we solve on a coarse grid, introducing large numerical diffusion, makes it even more striking that bimodal solutions are clearly evident in the solution. Grid refinement and more accurate numerical methods can be expected to emphasize the wave separation even more.

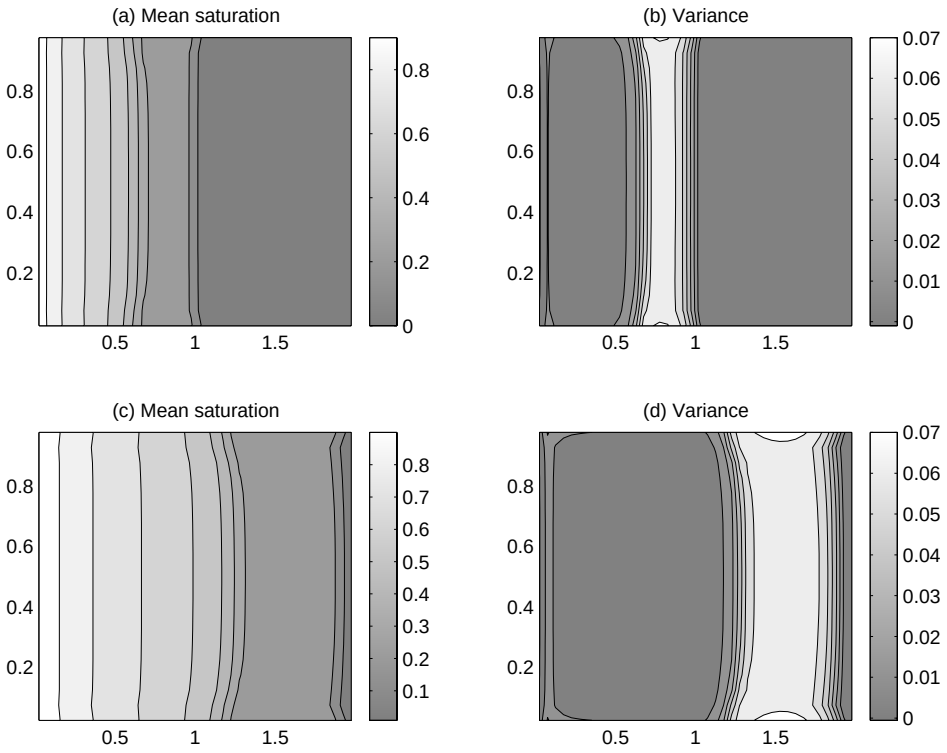

FIG. 4.3. *Saturation mean and variance contours at (a,b) early and (c,d) late times. Lighter shades indicate a higher mean water saturation or higher variance.*

The separation between wave fronts increases with time. In many specific applications the relevant time scale may be such that a separation is not evident; however, even when diffusion dominates initially, bimodality will appear over sufficiently long times. This property of the solution must be accounted for in any use of MDEs for advection and diffusion, for both single-phase and multiphase applications.

4.2. Comparison to MCS. Monte Carlo simulations are frequently used in applications to subsurface flow and transport and for reservoir modeling. The primary drawback is that MCS is computationally costly. Separate and very important issues include the problem of fair sampling of the true sample space and the standard problem of autocorrelation in random number generators. However, it is a well-established method and serves as a standard for comparison.

For a bound on the error $|\bar{s}(\mathbf{x},t) - \langle s \rangle (\mathbf{x},t)|$ of just 10^{-2}, we estimate that about 4000 simulations are needed. This is a significant burden on time and space resources, so we present results of only 350 simulations. This gives an estimated absolute error bound of about 0.032, which is sufficient for a rough comparison (recall that mean saturation values are restricted to $[0,1]$).

Local correlation structure is again evident in MCS velocity moments in Fig. 4.7 (compare to Fig. 4.2). Sample mean and an envelope of one standard deviation along the midline $x_2 = L_2/2$ are shown in Fig. 4.8. Contours of sample moments are shown in Fig. 4.9. The roughness of the contours highlights the fact that a greater number of simulations is required to obtain high accuracy. The mean front is near $x_1 = 1.3$,

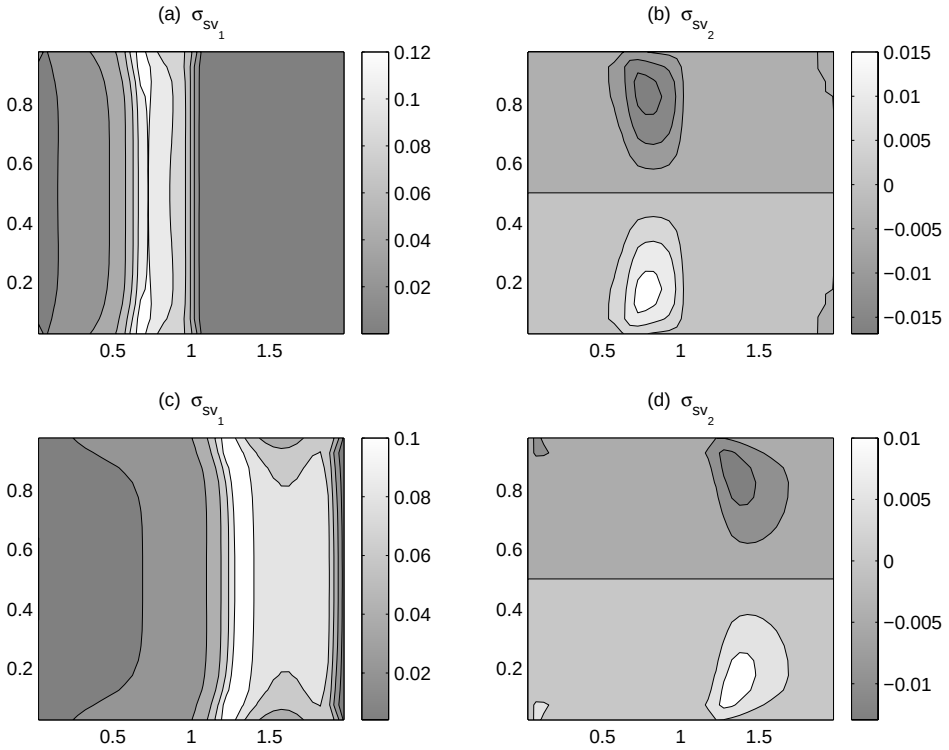

FIG. 4.4. *Saturation-velocity moments at (a,b) early and (c,d) late times.*

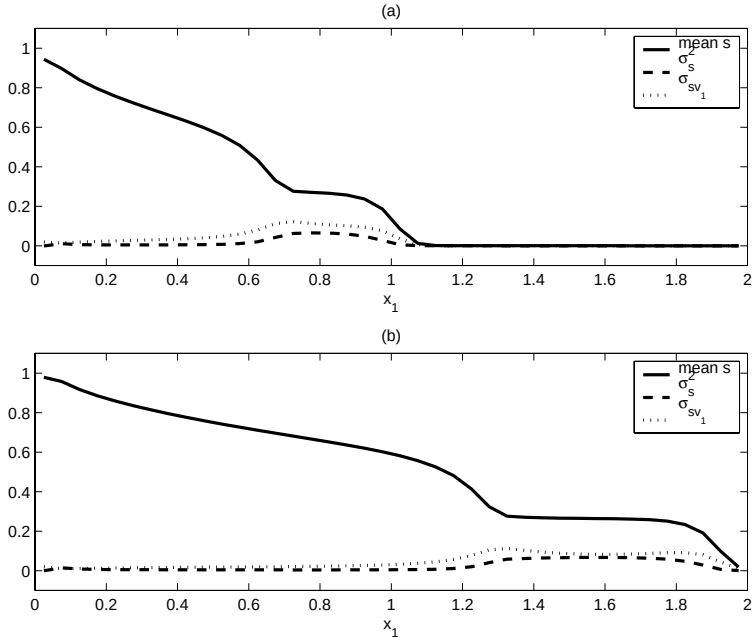

FIG. 4.5. *Saturation moment profiles at (a) early and (b) late times.*

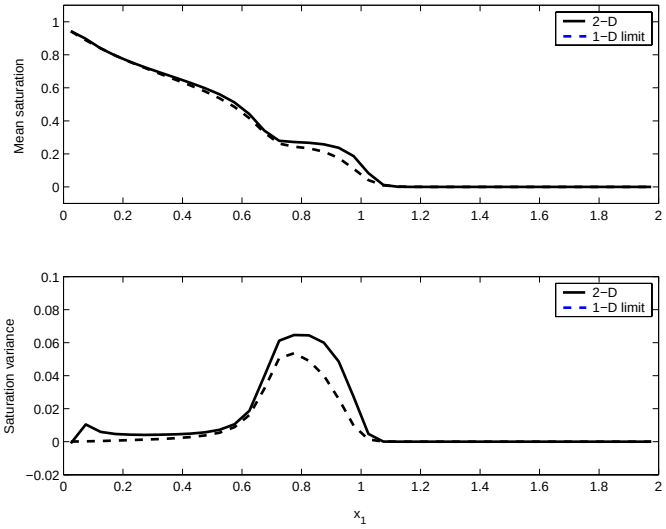

FIG. 4.6. *Comparison of 2-D and 1-D flow.*

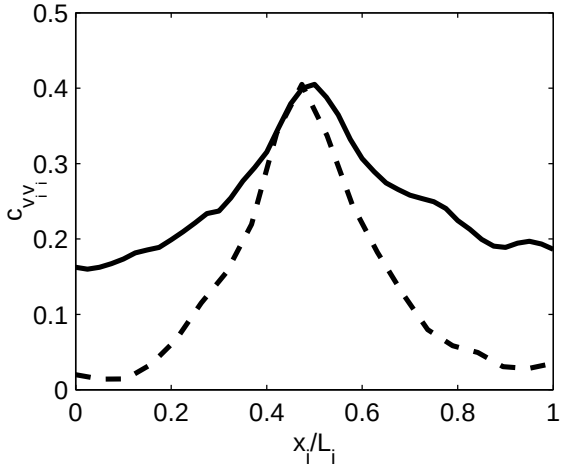

FIG. 4.7. *Sample velocity covariance $c_{v_1 v_1}$, showing finite correlation length. The solid line shows covariance between v_1 at the center of the domain and at all points along $x_2 = L_2/2$. The dotted line shows covariance between v_1 at the center and at all points along $x_1 = L_1/2$.*

where the variance is greatest.

To make the comparison between MCS and MDE as consistent as possible, the MDE solution is computed here using the sample velocity moments. This comparison isolates the difference between the two methods at the level of computing saturation moments (kindly suggested by Neuman and Guadagnini [24]). Contours of MDE solutions using MCS velocity moments are shown in Fig. 4.9, where they are compared to MCS saturation moments. A clearer comparison is seen in profiles of saturation moments in Fig. 4.10, which shows solutions at a late time along $x_2 = L_2/2$. Of

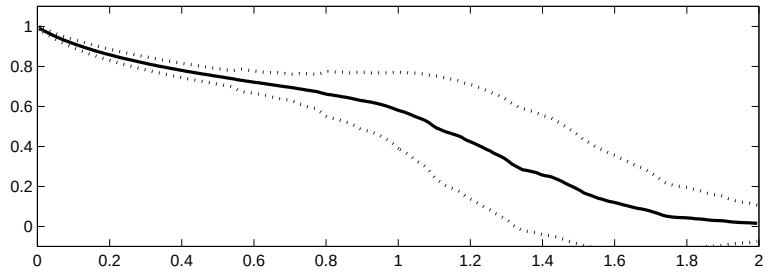

FIG. 4.8. *Saturation sample mean profile, with an envelope of one standard deviation.*

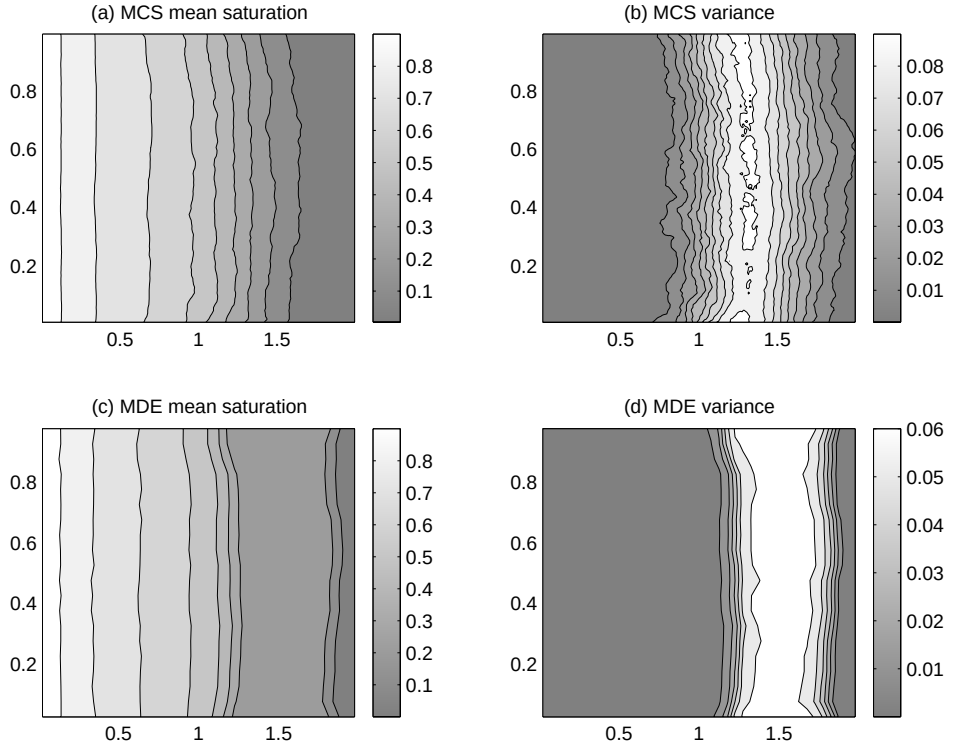

FIG. 4.9. *MCS saturation (a) mean and (b) variance and MDE (c) mean and (d) variance using MCS velocity moments.*

course, MCS and our MDE cannot match; there is no physical reason to expect that a bimodal solution can be obtained from simulations in our model. However, the MDE mean is centered near the simulation mean, and variances computed by both methods are similar. The MDE solution is ahead of the MCS solution, which is likely due to the effects of numerical and artificial diffusion. The first of these effects is much larger for MDE due to the coarse grid on which it is computed.

The comparison shows, not surprisingly, that the MDE moments are not an accurate representation of the details of MCS moments. They provide a useful first approximation, particularly if a rough estimate of the location and magnitude of uncertainty is sufficient in an application. The comparison is favorable in the rarefaction

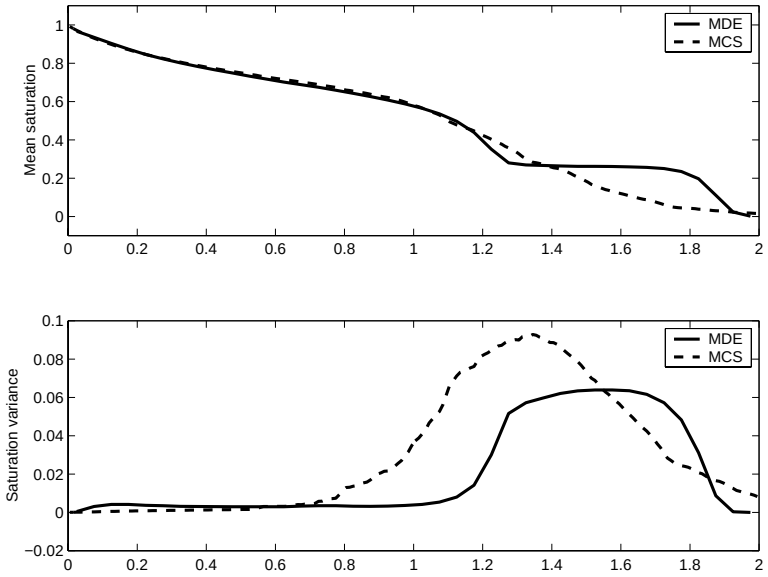

FIG. 4.10. *Comparison of MDE and MCS saturation moments.*

zone, but we are more concerned with behavior near the (true) mean saturation front. In 1-D, [18] explains the observed bimodality in terms of the eigenvalues and eigenvectors of the hyperbolic system of MDEs. This finite-dimensionality results from the truncation of the expansions in (2.3) and (2.4). We speculate that if more terms were retained, the number of modes would increase, but their magnitude would decrease, forming a closer representation of MCS moments.

For integrated or averaged quantities, the MDE estimates are better. For example, the solution does provide a good estimate of the total production, which is a key measure in the oil industry. The total oil produced is computed as the mass quantity that has exited the right boundary at time t. The volume of oil this represents is the same as the volume of water injected in this case, which is given by

$$P(t) \equiv \iint_A \phi\, s(\mathbf{x}, t) d\mathbf{A}, \tag{4.2}$$

(assuming unit domain length in the vertical and unit density of oil) in each simulation. Sample mean and variance of $P(t)$ are computed and compared to an estimate of mean production from MDE. The latter is obtained by replacing s in the integral with $\tilde{s}$. The results are shown in Fig. 4.11 (here only 200 simulations were used).

The curves are fairly closely matched; the MDE curve lies within one sample standard deviation $\bar{\sigma}_s$ of the MCS curve, except near $t = 0$. The MDE curve has two sharp changes in slope, which are due to the passing of the two saturation fronts through the right boundary. In each of the first two segments, the curve is nearly linear, which it should be for an intransient velocity field. Until water reaches the boundary (breakthrough), a constant flux of oil leaves the domain. The flux is again nearly constant between the saturation fronts, providing the second linear segment. Finally, after the second front passes the boundary, production decays smoothly as the rarefaction part of the mean saturation crosses.

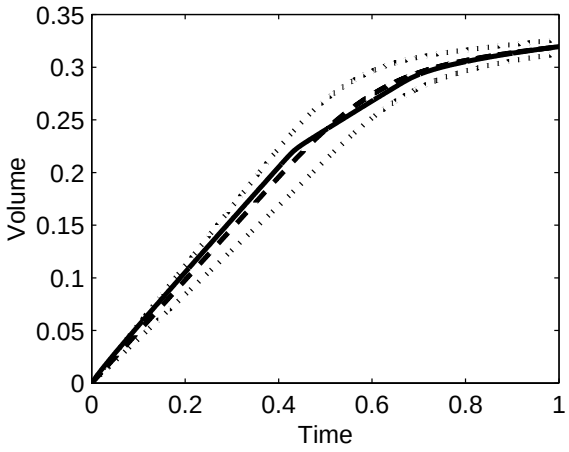

FIG. 4.11. *Total Production. Solid curve is obtained by MDE, dashed curve is MCS mean. One standard deviation is shown by dotted curves (200 samples).*

MCS provides solutions with high resolution; this is also a requirement, as the velocity field in each simulation may change significantly over short spatial scales. Averaging provides relatively smooth velocity and saturation moments. The MDE approach takes advantage of the smoothness of these moments before they are computed. Thus, we do not need a fine grid to capture detail. Grid refinement will certainly improve the solution to MDE, but refinement is not necessary to capture small-scale features.

We computed rough estimates of computational costs and found that on an SGI 300MHz MIPS12K processor with 256M memory, a set of 200 simulations on 200 by 100 grid nodes takes about 8 hours. To achieve an error tolerance of 10^{-2} (to within 97.5% confidence), we estimate that 4000 simulations are necessary, which would take about 160 hours on the same computer. This is much longer than the 5 hours it takes to obtain the solutions presented here using the MDE code. These are crude estimates; a careful comparison of costs for the two methods must allow for some attention to improving efficiency in both codes and should account for several differences between the methods, including the significantly higher storage cost for MDE. Additional details on the MCS approach we used can be found in Appendix B and in [16].

5. Conclusions. Bimodal moments are obtained for saturation in 2-D as in earlier results for 1-D, in spite of the finite length scale for velocity correlations in 2-D. The fact that velocity correlations lead to a macrodispersion term in lower-order approximations to moments would suggest a partial transition from hyperbolic to parabolic character as we move from 1-D to 2-D. However, in the example herein we limit the domain to ten correlation lengths (far from the ergodic regime) so that macrodispersion effects may be very limited.

The two-phase Eulerian MDEs presented here complement the traditional MCS approach. MDEs provide a first approximation to moments relatively quickly. Rather than compute several hundred sample saturation fields on fine grids and post-process to obtain moments, a single solution of MDEs is computed on a coarse grid. In spite of a non-physical bimodality in MDE moments, we obtain a good match between MDE

and MCS in the total oil production curve. For high accuracy, MCS is appropriate and, in real applications, it may be of most benefit to combine the two methods. It may also be possible to improve the accuracy of MDEs by retaining more terms in the perturbation expansions.

The Eulerian MDE approach applies to any probability distribution of geologic properties with any correlation function. It depends solely on moments rather than a particular probability distribution and does not require stationarity, thus removing restrictions that are common to stochastic subsurface theories.

6. Acknowledgments. We are grateful to Joseph Oliveira for many conversations on this topic.

Appendix A. Velocity moments from MDE.

Additional velocity moment profiles are shown in Fig. A.1 and Fig. A.2. These were obtained using the MDE flux code of Zhang and Winter [36]. The dominant component is longitudinal. Transverse flow is inward near the inflow (left) boundary, and outward near the outflow (right) boundary. Longitudinal flow is significantly greater along the sides, where transverse flux is zero.

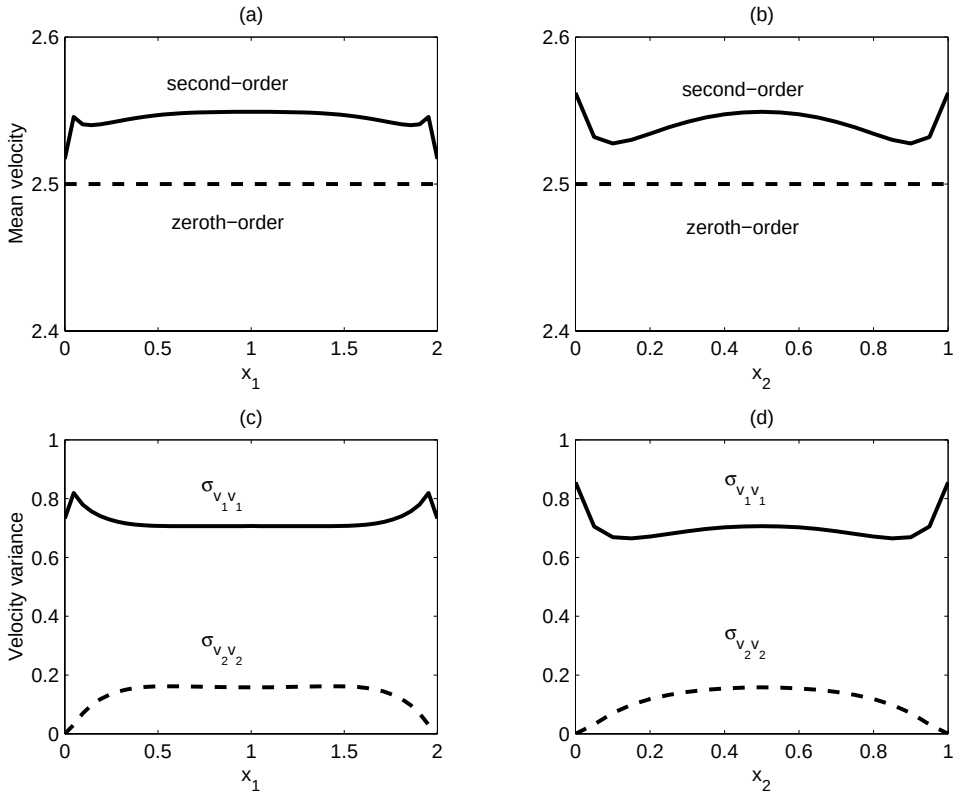

FIG. A.1. *Mean velocity estimates* $(v_0)_1$ *and* $\tilde{v}_1$ *at (a)* $x_2 = L_2/2$ *and (b)* $x_1 = L_1/2$*; velocity variances* $\sigma_{v_iv_i}$ *at (c)* $x_2 = L_2/2$ *and (d)* $x_1 = L_1/2$.

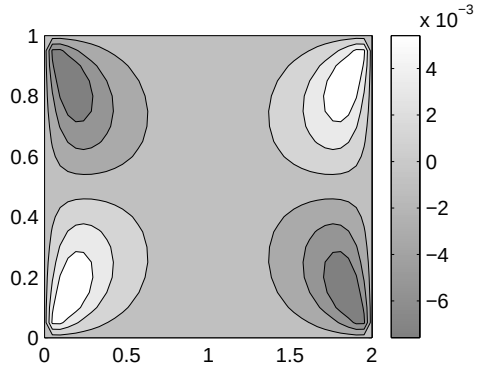

FIG. A.2. *Mean transverse velocity.*

Appendix B. MCS and convergence.

Monte Carlo simulations were performed by numerically solving the total velocity and saturation equations (1.1) and (1.2) over replicates of log hydraulic conductivity with correlation function (4.1). Replicates were generated with a Fast Fourier Transform algorithm developed by Gutjahr and colleagues [14]. Velocity equations were solved with a conjugate gradient algorithm. Saturation profiles were obtained using a first-order upwind approach just as for MDEs, also within the framework of CLAWPACK.

We performed simple tests for convergence of the mean and variance of saturation. A tolerance of approximately 0.032 to within 97.5% confidence is estimated for results of the 350 simulations presented here. Cumulative average saturation from the first 150 simulations at representative grid points is shown in Fig. B.1. Although it is well-known that convergence of such estimates may appear imminent when in fact they are not, this is still a useful tool. We may be reasonably confident in the simulation moments for comparison to MDE; however, it is clear from the figures in §4.2 that a larger number of simulations would be needed to obtain the smooth profiles we expect.

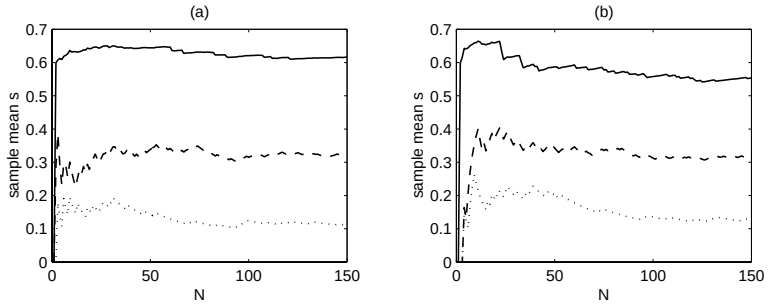

FIG. B.1. *Convergence of sample mean saturation at (a) $x_2 = 0.4$ and (b) $x_2 = 0.4$; in both, $x_1 = 1.2$ (solid), $x_1 = 0.95$ (dashed), and $x_1 = 0.7$ (dotted).*

REFERENCES

[1] M. B. Allen, G. A. Behie, and J. A. Trangenstein, *Multiphase Flow in Porous Media*, vol. 34 of Lecture Notes in Engineering, Springer, 1988.
[2] O. Amir and S. Neuman, *Gaussian closure of one-dimensional unsaturated flow in randomly heterogeneous soils*, Transp. Porous Media, 44 (2001), pp. 355–383.
[3] J. Bear, *Dynamics of Fluids in Porous Media*, Elsevier, New York, 1972.
[4] V. Cvetkovic, A. Shapiro, and G. Dagan, *A solute flux approach to transport in heterogeneous formations 2. Uncertainty analysis*, Water Resour. Res., 28 (1992), pp. 1377–1388.
[5] G. Dagan, *Flow and Transport in Porous Formations*, Springer, 1989.
[6] G. Dagan and V. Cvetkovic, *Reactive transport and immiscible flow in geological media. I. General theory*, Proc. R. Soc. Lond. A, 452 (1996), pp. 285–301.
[7] G. Dagan, V. Cvetkovic, and A. Shapiro, *A solute flux approach to transport in heterogeneous formations 1. The general framework*, Water Resour. Res., 28 (1992), pp. 1369–1376.
[8] G. de Marsily, *Quantitative Hydrogeology: Groundwater Hydrology for Engineers*, Academic Press, New York, 1986.
[9] D. W. Dean, *An analysis of the stochastic approaches to the problems of flow and transport in porous media*, PhD thesis, University of Colorado, Boulder, 1997.
[10] J. P. Delhomme, *Spatial variability and uncertainty in groundwater flow parameters: A geostatistical approach*, Water Resour. Res., 15 (1979), pp. 269–280.
[11] R. A. Freeze, *A stochastic-conceptual analysis of one-dimensional groundwater flow in nonuniform homogeneous media*, Water Resour. Res., 11 (1975), pp. 725–741.
[12] L. W. Gelhar, *Stochastic Subsurface Hydrology*, Prentice–Hall, Englewood Cliffs, NJ, 1993.
[13] W. Graham and D. McLaughlin, *Stochastic analysis of nonstationary subsurface solute transport 1. Unconditional moments*, Water Resour. Res., 25 (1989), pp. 215–232.
[14] A. Gutjahr, B. Bullard, and S. Hatch, *General joint conditional simulations using a Fast Fourier Transform method*, Math. Geol., 29 (1997), pp. 361–389.
[15] J. O. Hinze, *Turbulence*, Mechanical Engineering, McGraw–Hill, New York, second ed., 1975.
[16] K. D. Jarman, *Stochastic Immiscible Flow with Moment Equations*, PhD thesis, University of Colorado, 2000.
[17] K. D. Jarman and T. F. Russell, *Comparison of perturbation techniques for stochastic two-phase flow.* in preparation.
[18] ———, *Moment equations for stochastic immiscible flow.* submitted.
[19] P. Langlo and M. S. Espedal, *Heterogeneous reservoir models, Two-phase immiscible flow in 2-D*, in Comput. Methods in Water Resources, vol. 9, Elsevier, New York, 1992, pp. 71–79.
[20] ———, *Macrodispersion for two-phase, immiscible flow in porous media*, Adv. in Water Resour., 17 (1994), pp. 297–316.
[21] R. J. Leveque, *CLAWPACK Version 4.0 User's Guide*, University of Washington, rjl@amath.washington.edu, August 1999.
[22] J. L. Lumley and H. A. Panofsky, *The Structure of Atmospheric Turbulence*, vol. 12 of Monographs and Texts in Physics and Astronomy, Wiley, 1964.
[23] S. P. Neuman, *Eulerian-Lagrangian theory of transport in space-time nonstationary velocity fields: Exact nonlocal formalism by conditional moments and weak approximation*, Water Resour. Res., 29 (1993), pp. 633–645.
[24] S. P. Neuman and A. Guadagnini, 2000. Personal communication.
[25] C. S. Simmons, *A stochastic-convective transport representation of dispersion in one-dimensional porous media systems*, Water Resour. Res., 18 (1982), pp. 1193–1214.
[26] C. S. Simmons, T. R. Ginn, and B. D. Wood, *Stochastic-convective transport with nonlinear reaction: Mathematical framework*, Water Resour. Res., 31 (1995), pp. 2675–2688.
[27] J. Smoller, *Shock Waves and Reaction-Diffusion Equations*, Comprehensive Studies in Mathematics, Springer, 1983.
[28] D. M. Tartakovsky and S. P. Neuman, *Transient flow in bounded randomly heterogeneous domains 1. Exact conditional moment equations and recursive approximations*, Water Resour. Res., 34 (1998), pp. 1–12.
[29] A. F. B. Tompson and L. W. Gelhar, *Numerical simulation of solute transport in three-dimensional, randomly heterogeneous porous media*, Water Resour. Res., 26 (1990), pp. 2541–2562.
[30] D. Zhang, *Numerical solutions to statistical moment equations of groundwater flow in nonstationary, bounded, heterogeneous media*, Water Resour. Res., 34 (1998), pp. 529–538.
[31] ———, *Nonstationary stochastic analysis of transient unsaturated flow in randomly heterogeneous media*, Water Resour. Res., 35 (1999), pp. 1127–1141.
[32] ———, *Quantification of uncertainty for fluid flow in heterogeneous petroleum reservoirs*, Physica D, 133 (1999), pp. 488–497.
[33] ———, *Stochastic Methods for Flow in Porous Media: Coping with Uncertainties*, Academic

Press, 2001.
[34] D. Zhang and H. Tchelepi, *Stochastic analysis of immiscible two-phase flow in heterogeneous media*, Soc. Pet. Eng. J., (1999). SPE#59250.
[35] D. Zhang, H. Tchelepi, and L. Li, *Stochastic formulation for uncertainty assessment of two-phase flow in heterogeneous reservoirs*, in 1999 SPE Reservoir Simulation Symposium, Society of Petroleum Engineers, February 1999, pp. 389–402. SPE#51930.
[36] D. Zhang and C. L. Winter, *Moment-equation approach to single phase fluid flow in heterogeneous reservoirs*, Soc. Pet. Eng. J., 4 (1999).